Universality of Local Dissipation Scales in Buoyancy-Driven Turbulence

Quan Zhou[1,2] and Ke-Qing Xia[1]

[1]Department of Physics, The Chinese University of Hong Kong, Shatin, Hong Kong, China
[2]Shanghai Institute of Applied Mathematics and Mechanics, Shanghai University, Shanghai 200072, China

(Received 11 November 2009; published 26 March 2010)

We report an experimental investigation of the local dissipation scale field η in turbulent thermal convection. Our results reveal two types of universality of η. The first one is that, for the same flow, the probability density functions (PDFs) of η are insensitive to turbulent intensity and large-scale inhomogeneity and anisotropy of the system. The second is that the small-scale dissipation dynamics in buoyancy-driven turbulence can be described by the same models developed for homogeneous and isotropic turbulence. However, the exact functional form of the PDF of the local dissipation scale is not universal with respect to different types of flows, but depends on the integral-scale velocity boundary condition, which is found to have an exponential, rather than Gaussian, distribution in turbulent Rayleigh-Bénard convection.

DOI: 10.1103/PhysRevLett.104.124301 PACS numbers: 44.25.+f, 47.27.eb

Fluid turbulence exhibits an intermittent nature ubiquitously, such as intense spikes of velocity gradients and energy dissipation rates in both space and time. Such behavior is usually studied quantitatively by investigating the cascades of turbulent kinetic energy transferred continuously from large to small scales [1–3]. In the classical Kolmogorov theory [4], this cascade process would stop at the smallest length scale of turbulence, known as the Kolmogorov dissipation scale η_K, below which energy is dissipated into heat. Based on dimensional arguments, η_K can be derived as $\eta_K = (\nu^3/\langle\epsilon\rangle)^{1/4}$, where ν is the kinematic viscosity of the fluid. As a mean length obtained from the mean energy dissipation rate $\langle\epsilon\rangle$, however, η_K precludes the intermittent nature of turbulence. To establish a connection between the dissipation scale and the intensive and localized turbulent events, Paladin and Vulpiani [5] put forward the idea of a local dissipation scale; i.e., the local Reynolds number associated with an eddy of length scale η is of order 1: $\mathrm{Re}_\eta = \eta|\delta_\eta v|/\nu \sim 1$. Here, $\delta_\eta v = v_r(r+\eta) - v_r(r)$ is the longitudinal velocity increment over a separation η. Such a definition implies a local balance between the inertial force $(\delta_\eta v)^2/\eta$ and the viscous force $\nu|\delta_\eta v|/\eta^2$ at a particular point in space and time. The resulting η is therefore a field that fluctuates in both space and time and hence may be used to reflect intermittency. Recently, the probability density function (PDF) of η, $Q(\eta)$, within the range $0 < \eta < L$ (L is the integral length scale of the turbulence) was proposed analytically by Yakhot [6,7] based on the Mellin transform of structure functions and by Biferale [8] based on the multifractal formalism. Both analytical predictions consist of distributions of scales varying from very fine sub-Kolmogorov scales, related to the very intense velocity gradients in the form of slender vortex filaments with diameters of order η_K or even less, to those much larger than η_K. Results obtained later from high-resolution numerical simulations of homogeneous and isotropic box turbulence [9,10] and experiments in turbulent pipe flows [11] were both found to agree well with the theoretical distributions. These results seem to suggest a universality of the smallest-scale fluctuations around η_K, but further tests in different types of turbulent flows are needed.

In this Letter we want to generalize these ideas into buoyancy-driven turbulence, an important class of turbulent flows that plays an essential role in many natural processes. The flow at hand is turbulent convection in a fluid layer heated from below and cooled on the top, i.e., turbulent Rayleigh-Bénard convection (RBC), which has become a paradigm for understanding buoyancy-driven turbulence [12,13]. Cascades of velocity and temperature fluctuations in such a system have been studied extensively in the past two decades [13]. Here, we report measurements of the local dissipation scale distribution at three representative locations in the convection cell. The convection cell is similar to that used in previous experiments [14], but has a different size. Briefly it is a vertical cylinder with top and bottom copper plates and Plexiglas sidewall, with its height H and inner diameter both being 50 cm. The experiment was conducted at fixed Prandtl number $\mathrm{Pr} = \nu/\kappa = 5.5$ and covered the range $5.9 \times 10^9 \lesssim \mathrm{Ra} \lesssim 1.1 \times 10^{11}$ of the Rayleigh number $\mathrm{Ra} = \alpha g \Delta T H^3/\nu\kappa$, with g being the gravitational acceleration, ΔT the temperature difference across the fluid layer, and α and κ being, respectively, the thermal expansion coefficient and the thermal diffusivity of the working fluid (water). The velocity field was measured by the particle image velocimetry (PIV) technique with a measuring area of 3.7×3.7 cm^2 and a spatial resolution $\Delta_l = 0.59$ mm, corresponding to 63×63 measured velocity vectors. Hollow glass spheres of 10-μm diameter were used as seed particles. The PIV measurements were performed at three different places of the cell: its center, 2 cm from the side-

wall at midheight, and 2 cm above the center of the bottom plate. The horizontal velocity component $u(x, z)$ and the vertical one $w(x, z)$ were obtained in the laser-illuminated vertical plane of the large-scale circulation, denoted as the xz plane. Each measurement lasted 3 hours in which a total of 25 000 two-dimensional vector maps were acquired with a sampling rate $\sim$2.3 Hz.

The PDF $Q(\eta)$ is determined from the measured velocity fields in the following way. We first fix a length ℓ that is an integral multiple of the spatial resolution Δ_l, i.e. $\ell = n\Delta_l$. The longitudinal velocity increments across the separation ℓ in both horizontal and vertical directions, $\delta_\ell u$ and $\delta_\ell w$, are then calculated for each velocity vector measured at each discrete time t. If either of the obtained values of $\ell|\delta_\ell u|/\nu$ and $\ell|\delta_\ell w|/\nu$ is between 0.9 and 2 [11], it contributes to the occurrence of local dissipation at a scale $\ell = \eta$. $Q(\eta)$ is then determined as $Q(\eta) = qn(\eta)/N(\eta)$, where $N(\eta)$ is the total number of calculated velocity increments over a separation η, $n(\eta)$ is the count of events among $N(\eta)$ that satisfy the local balance at scale η, and q is a normalization parameter determined from $\int Q(\eta)d\eta = 1$. In the following, three PDFs are presented. $Q(\eta^x)$ is obtained from the u component only and $Q(\eta^z)$ from the w component only, whereas, $Q(\eta)$ contains contributions from both the horizontal and vertical velocity components.

Figures 1(a) and 1(b) show log-log plots of $Q(\eta^x/\eta_0)$ (open circles) and $Q(\eta^z/\eta_0)$ (solid triangles) measured at the three locations. Here, the results have been rescaled by $\eta_0 = L\mathrm{Re}_L^{-0.72}$ [10], where Re_L is the Reynolds number based on the integral length scale. One sees that at each measuring location the distributions obtained in horizontal and vertical directions coincide excellently with each other within all measured scales, suggesting that the turbulent dynamics of the dissipative range in buoyancy-driven turbulence is isotropic. As the flow is driven by buoyancy in the vertical direction, this result is somewhat unexpected and surprising, especially for data obtained in the plume-dominated regions near the sidewall and near the bottom plate where the turbulent flows are highly anisotropic. The results shown in Fig. 1 reveal that such buoyancy-induced anisotropy cannot be differentiated by $Q(\eta^x)$ and $Q(\eta^z)$ for velocity components measured along different directions. Hereafter, we will discuss only measured $Q(\eta)$.

Figure 1(c) shows $Q(\eta/\eta_0)$ for all values of Ra. The figure appears to show that the shape of $Q(\eta)$ is independent of Ra. However, as we shall see below, predictions of theoretical models, i.e., Eqs. (1) and (2), both show a dependence on Re_L (thus Ra). This is because comparing to the dependence on η, the dependence on Re_L is weak and over the parameter range of our experiment this weak Re_L dependence cannot be manifested clearly in the measured $Q(\eta)$. With the measured $Q(\eta/\eta_0)$, one can estimate a mean dissipation scale from its first moment. Here, we find that $\langle\eta\rangle = 7.1\eta_0$, $7.7\eta_0$, and $8.1\eta_0$ for distributions obtained at cell center, near the sidewall, and near the bottom plate, respectively. These mean values of η are close to $10\eta_K$, which is located at the lower end of the inertial range [15,16]. Note that because of the limited resolution our present results could not properly resolve the left tail of $Q(\eta/\eta_0)$ when $\mathrm{Ra} \gtrsim 5.7 \times 10^{10}$ [Fig. 1(b)].

In Fig. 2, we compare $Q(\eta/\eta_0)$ measured at the three representative locations: at nearly homogeneous and isotropic cell center (circles) and in the plume-dominated regions near the sidewall (up triangles) and near the bottom plate (down triangles). It is seen that the three distributions are nearly identical with each other. This suggests that $Q(\eta/\eta_0)$ is insensitive to the large-scale inhomogeneity of turbulent RBC, further indicating the universality of $Q(\eta/\eta_0)$ (for the same type of flow). Nevertheless, one can also see that $Q(\eta/\eta_0)$ measured in the plume-dominated regions exhibit a less-steep left tail than that measured at cell center. An increase of the probabilities at the smallest values of η/η_0 indicates the enhanced velocity gradients at these scales and hence is a manifestation of the increased level of small-scale intermittency. As the Reynolds number dependence of $Q(\eta/\eta_0)$ is weak, this feature could be attributed to the presence of coherent

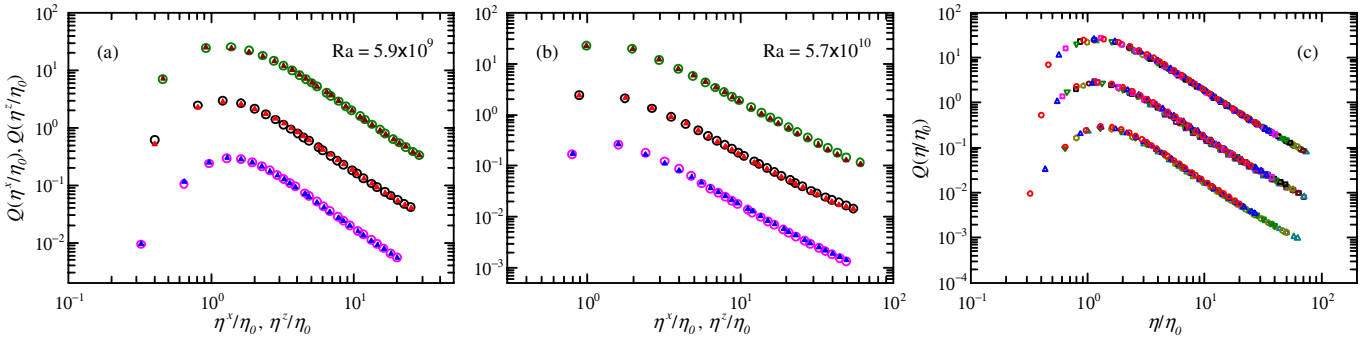

FIG. 1 (color online). (a),(b) PDFs of the local dissipation scales for the horizontal and vertical velocity components, $Q(\eta^x/\eta_0)$ (open circles) and $Q(\eta^z/\eta_0)$ (solid triangles), measured at different locations and for different Ra. (c) The measured $Q(\eta/\eta_0)$ for various values of Ra. For clarity, in (a), (b), and (c) results obtained near the sidewall and near the bottom plate are shifted upwards by one and two decades, respectively, with respect to those obtained at cell center.

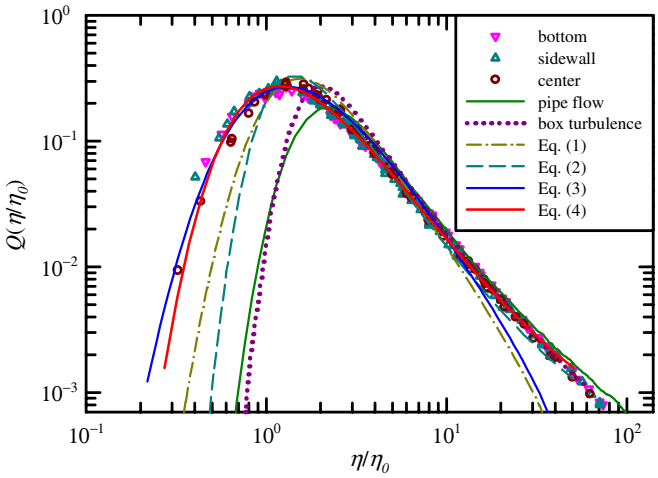

FIG. 2 (color online). Comparison among $Q(\eta/\eta_0)$ measured at the three representative locations in the cell for all values of Ra, the experimental result from turbulent pipe flow [11], the numerical result for box turbulence [10], and the theoretical distributions according to Eqs. (1)–(4) obtained with $\mathrm{Re}_L = 217$ (the Reynolds number obtained at cell center for $\mathrm{Ra} = 1.1 \times 10^{10}$).

structures, like plumes, in the near-wall regions. In the figure, numerical and experimental data from homogeneous isotropic box turbulence [10] and from turbulent pipe flows [11] are also shown. (The two data sets were both taken from Fig. 4 of Ref. [11] using data capturing software.) Good agreements can be seen in the right tails, whereas, for the left tail at small η, our results exhibit much higher probabilities. This suggests a much higher level of small-scale intermittency possessed by our thermal turbulence in comparison to those of box turbulence and turbulent pipe flows, although the nominal Reynolds numbers for our flow are comparable or even smaller than the latter two cases. This may be understood by the presence of thermal plumes, which have a characteristic dimension of thermal boundary layer that is smaller than η_K.

The theoretical $Q(\eta)$ can be derived in several ways. Using the Mellin transform of structure functions, Yakhot [6] showed that

$$Q(\eta) = 2/\{\pi\eta[b\log(L/\eta)]^{1/2}\}\int_0^\infty dx \times \exp\left[-x^2 - \frac{\{\log[\frac{\sqrt{2}x\mathrm{Re}_L}{c}(\frac{\eta}{L})^{a+1}]\}^2}{4b\log(L/\eta)}\right], \quad (1)$$

within the range $0 < \eta < L$, where $a = 0.383$, $b = 0.0166$, and $c = O(1)$ is a fitting parameter [10,11]. Based on the multifractal formalism, Biferale [8] obtained

$$Q(\tilde{\eta}) = \int dh A^{4-h-D(h)}\mathrm{Re}_L^{[3h+3D(h)-10]/4}\tilde{\eta}^{1-h-D(h)} \times \exp[-0.5A^{2(1-h)}\mathrm{Re}_L^{(3h-1)/2}\tilde{\eta}^{-2(1+h)}], \quad (2)$$

where $A = O(1)$ is a fitting parameter, h is the local scaling (or Hölder) exponent, $D(h)$ is the multifractal dimension spectrum, and $\tilde{\eta} = \eta/\eta_K$ with $\eta_K = L\mathrm{Re}_L^{-3/4}$ [17]. In Fig. 2 we compare directly the theoretical $Q(\eta/\eta_0)$ according to Eqs. (1) and (2) with our measured results [18]. Here we see that our measured $Q(\eta)$ have much higher values at small η than both theoretical predictions.

To understand such a discrepancy, we note that both theoretical approaches [6,8] use the assumption that velocity increments $\delta_L v$ across the integral length scale L are Gaussian distributed, i.e. $P(\delta_L v) \sim \exp(-\delta_L v^2/2)$. Specifically, in Eq. (2), the left tail of $Q(\eta)$ is dominated by contributions from the stretched exponential in that equation, which stems from the Gaussian-distributed integral-length-scale velocity. However, the assumption of Gaussianity has not been verified in the present system. To test this, we measured the global velocity field over an area of 49×49 cm^2 ($\Delta_\ell = 7.76$ mm) in the convection cell using the PIV method and obtained the integral-scale velocity increments at the three locations. Figure 3 shows the PDFs of $\delta_L w$ at cell center and near the sidewall and that of $\delta_L u$ near the bottom plate. One finds surprisingly that the measured PDFs exhibit decaying exponential tails at all three locations, rather than Gaussian distribution (dashed curve in the figure). This is different from all known experiments and simulations of isotropic turbulence. To offer a plausible explanation, we note that the turbulent flow in our system is driven by buoyancy in the vertical direction, which is also believed to be the dominant force governing the cascade dynamics above the so-called Bolgiano scale [13]. In the time domain, it has been found that the Bolgiano time scale in turbulent RBC is of order 1 s [19–21], which is only a factor of 2 or 3 smaller than the integral time scale. The observed exponential distributions

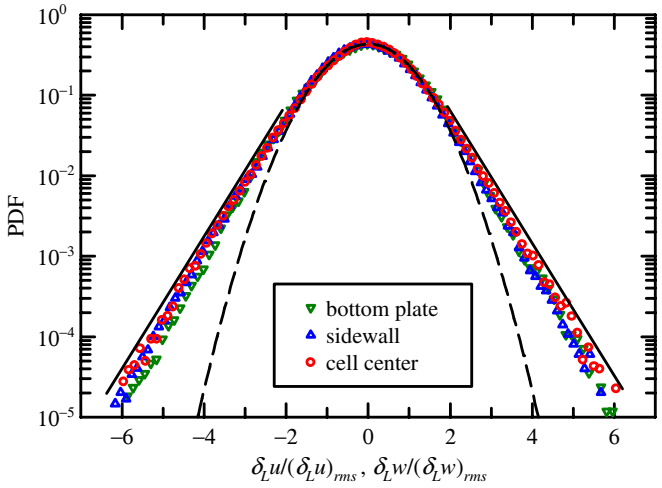

FIG. 3 (color online). PDFs of the vertical velocity increments $\delta_L w$ at cell center (circles) and near the sidewall (up triangles) and that of the horizontal velocity increments $\delta_L u$ near the bottom plate (down triangles) at $\mathrm{Ra} = 9.5 \times 10^{10}$ and $\mathrm{Pr} = 5.5$. The dashed line is a Gaussian distribution for reference.

of $\delta_L u$ and $\delta_L w$ may thus come from the buoyancy-induced intermittency, which is then transferred from large to small scales.

Motivated by the distributions revealed by Fig. 3, we now modify the two models proposed by Yakhot and Biferale, respectively. Following the same derivations as in Refs. [6,8], but instead using the exponential distribution $P(\delta_L v) \sim \exp(-|\delta_L v|)$ for the integral-length-scale velocity increments, we obtain, respectively,

$$Q(\eta) = 1/\{\eta[b\pi \log(L/\eta)]^{1/2}\} \int_0^\infty dx \times \exp\left[-x - \frac{\{\log[\frac{x\mathrm{Re}_L}{c}(\frac{\eta}{L})^{a+1}]\}^2}{4b\log(L/\eta)}\right], \quad (3)$$

and

$$Q(\tilde{\eta}) = \int dh A^{4-h-D(h)} \mathrm{Re}_L^{[3h+3D(h)-10]/4} \tilde{\eta}^{1-h-D(h)} \times \exp[-A^{(1-h)} \mathrm{Re}_L^{(3h-1)/4} \tilde{\eta}^{-(1+h)}]. \quad (4)$$

Figure 2 shows direct comparison of $Q(\eta/\eta_0)$ according to Eqs. (3) (blue solid line) and (4) (red solid line) and our measured results. Excellent agreements between the experimental and theoretical results for nearly all measured η can be seen, except for Eq. (3) at large η. These excellent agreements with both predictions suggest that the models developed for isotropic and homogeneous turbulence can also be applied to buoyancy-driven turbulence, like turbulent RBC. It is in this sense that our results reveal that the local dissipation scale dynamics is universal, whereas the exact functional form of the local dissipation scale PDF (specifically, its left part) depends on the integral-scale velocity boundary condition.

It is a pleasure to acknowledge helpful discussions with L. Biferale and J. Schumacher. We also thank J. Schumacher for his help in the derivation of Eq. (3). This work was supported by the Research Grants Council of Hong Kong SAR (No. CUHK403806 and No. CUHK403807). Q. Z. thanks the support of Innovation Foundation of Shanghai University, Shanghai NSF (No. 09ZR1411200), Chenguang Project (No. 09CG41), and RFDP of Ministry of Education of China (No. 20093108120007).

[1] U. Frisch, *Turbulence: The Legacy of A. N. Kolmogorov* (Cambridge Univ. Press, Cambridge, 1995).
[2] K. R. Sreenivasan and R. A. Antonia, Annu. Rev. Fluid Mech. **29**, 435 (1997).
[3] T. Ishihara, T. Gotoh, and Y. Kaneda, Annu. Rev. Fluid Mech. **41**, 165 (2009).
[4] A. N. Kolmogorov, Dokl. Akad. Nauk SSSR **30**, 301 (1941).
[5] G. Paladin and A. Vulpiani, Phys. Rev. A **35**, 1971 (1987).
[6] V. Yakhot, Physica (Amsterdam) **215**, 166D (2006).
[7] V. Yakhot, J. Fluid Mech. **606**, 325 (2008).
[8] L. Biferale, Phys. Fluids **20**, 031703 (2008).
[9] J. Schumacher, K. R. Sreenivasan, and V. Yakhot, New J. Phys. **9**, 89 (2007).
[10] J. Schumacher, Europhys. Lett. **80**, 54 001 (2007).
[11] S. C. C. Bailey, M. Hultmark, J. Schumacher, V. Yakhot, and A. J. Smits, Phys. Rev. Lett. **103**, 014502 (2009).
[12] G. Ahlers, S. Grossmann, and D. Lohse, Rev. Mod. Phys. **81**, 503 (2009).
[13] D. Lohse and K.-Q. Xia, Annu. Rev. Fluid Mech. **42**, 335 (2010).
[14] C. Sun, L.-Y. Ren, H. Song, and K.-Q. Xia, J. Fluid Mech. **542**, 165 (2005).
[15] C. Sun, Q. Zhou, and K.-Q. Xia, Phys. Rev. Lett. **97**, 144504 (2006).
[16] Q. Zhou, C. Sun, and K.-Q. Xia, J. Fluid Mech. **598**, 361 (2008).
[17] In the evaluations of Eqs. (2) and (4), the log-Poisson spectrum [Z.-S. She and E. Leveque, Phys. Rev. Lett. **72**, 336 (1994)], $D(h) = 3(h - \frac{1}{9})/\log(\frac{2}{3})[\log\{3(\frac{1}{9} - h)/2\log(\frac{2}{3})\} - 1] + 1$, was chosen and the integral was evaluated over the range $h_{\min} < h \leq h_{\max}$, where $h_{\min} = \frac{1}{9}$ and $h_{\max} = 0.38$ is obtained such that $D(h)$ reaches its maximum value of 3 at $h = h_{\max}$.
[18] Note that the parameters A and c essentially control the peak position of the theoretically-predicted $Q(\eta)$, in the two models, respectively. Here, we choose $A = 4$ and $c = 2$ to fit our experimental results. If different values of A and c were chosen, the predictions of the two models would fit the data of turbulent pipe flow and box turbulence much better than they appear in Fig. 2 (see, e.g., [8,10,11]). These fittings are not shown here to avoid overcrowding the figure and also because the purpose here is to compare the theoretical predictions with our measured data.
[19] S.-Q. Zhou and K.-Q. Xia, Phys. Rev. Lett. **87**, 064501 (2001).
[20] E. S. C. Ching, K. W. Chui, X.-D. Shang, X.-L. Qiu, P. Tong, and K.-Q. Xia, J. Turbul. **5**, 27 (2004).
[21] Q. Zhou and K.-Q. Xia, Phys. Rev. E **77**, 056312 (2008).